ISBN: 978-3-95450-249-3 ISSN: 2673-5350 doi: 10.18429/JACoW-IBIC2024-WEAI2

REMOTE SENSING OF FAST BEAM SIGNALS USING ELECTRO-OPTICAL MODULATORS

A. Schlögelhofer*, T. Lefèvre, T.E. Levens, S. Mazzoni, CERN, Geneva, Switzerland

Abstract

Electrical measurements of fast signals, as generated in particle accelerators, encounter severe limitations due to the high-frequency losses in radio frequency transmission lines. This study describes measurements conducted with electro-optical modulators employing various radio-over-fibre techniques. Experimental data consist of different beam-generated signals, which underline the versatility of such a system. Signals from electromagnetic devices such as wall current monitors, as well as those captured from coherent transition radiation screens and coherent Cherenkov diffraction radiators, are presented. Furthermore, the potential deployment of such a remote sensing acquisition system in large-scale facilities is discussed.

INTRODUCTION

In many particle accelerators, particle acceleration is achieved through the use of radio frequency (RF) cavities. This method forces the particles to form a train of particle bunches, resembling the structure of the accelerating RF field. As particle energies increase, the bunches become compressed in the longitudinal direction, which in turn extends bunch-induced signals to higher frequencies. Acquiring these high-frequency signals poses several challenges. Long transmission lines cause significant attenuation of the high-frequency components of the RF signals. The need for short transmission lines implicates dedicated development of radiation-hardened electronics, as most often radiation levels in the accelerator hall are not negligible. In this work, we address these challenges by employing various radio-over-fibre techniques for the transmission of beam-generated signals. We utilise Mach-Zehnder electro-optical modulators (Exail NIR-MX800-LN-20) to modulate the intensity of the optical carrier with the beam-induced electrical signals. By encoding these signals onto an optical carrier, we achieve transmission bandwidths of several tens of GHz over distances of hundreds of meters, enabling real-time, high-bandwidth measurements which are resistant to electromagnetic interference.

ELECTRO-OPTICAL MODULATOR

A Mach-Zehnder-type electro-optical modulator is an interferometric device that operates based on the Pockels effect in electro-optical crystals. The Pockels effect refers to the linear change of the refractive index of a material when exposed to an external electric field. For Lithium Niobate ($LiNbO_3$) crystals, which are used in this work, the Pockels effect is described by [1]

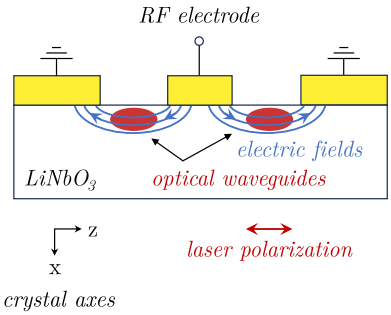

Figure 1: Schematic cross-section of an x-cut Mach-Zehnder type electro-optical modulator [2]. The RF input generates electric fields that alter the effective refractive index of the Lithium niobate ($LiNbO_3$) crystal, introducing a phase delay between the two interferometer arms (optical waveguides). The recombination of the light from both arms results in the modulation of the laser light intensity.

$$\Delta n_z = -\frac{1}{2} n_e^3 r_{33} E_z, \tag{1}$$

where Δn_z is the change of refractive index in z-direction, n_e is the extraordinary refractive index, r_{33} is an electro-optic coefficient of the electro-optic tensor of $LiNbO_3$, and E_z is the external field applied in z-direction. A schematic of the geometry used in x-cut Mach-Zehnder electro-optical modulators is shown in Fig. 1. The electric field lines overlap with the optical waveguides on either side, resulting in a symmetric design where the induced change in refractive index is positive in one arm and negative in the other.

After passing through the two modulator arms, the light is recombined, experiencing either constructive or destructive interference depending on the relative change in optical path length between the two interferometer arms. This phase modulation results in an intensity variation of the light at the output, which is why this type of electro-optical modulator is often referred to as an intensity modulator. The transfer function T of an ideal intensity modulator can be described as [2]

$$T(V) = \sin^2\left(\frac{\pi\,(V - V_0)}{2\,V_\pi}\right), \tag{2}$$

where V is the modulating voltage amplitude, V_0 is the bias voltage amplitude and V_π is the voltage required to transition from minimum to maximum transmission. The transfer function $T(V)$ is illustrated in Fig. 2 along with an electrical input signal and the corresponding optical output signal. Typically V_0 is a DC voltage chosen in such a way, that with $V = 0$ the optical transmission is at 50% of its total intensity. This is referred to as the quadrature point of the modulator (indicated by the yellow marker in Fig. 2). Any variation in $V = V_{RF}$ modulates the optical intensity relative

* andreas.schloegelhofer@cern.ch

ISBN: 978-3-95450-249-3 ISSN: 2673-5350 doi: 10.18429/JACoW-IBIC2024-WEAI2

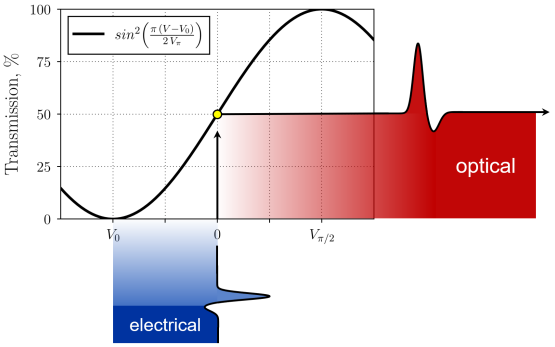

Figure 2: Schematic of the transfer function of an intensity modulator. The bias voltage V_0 is selected to position the transfer function at a constant 50 % transmission level. The fast RF signal is then superimposed, utilising the linear portion of the sin^2-function for modulation.

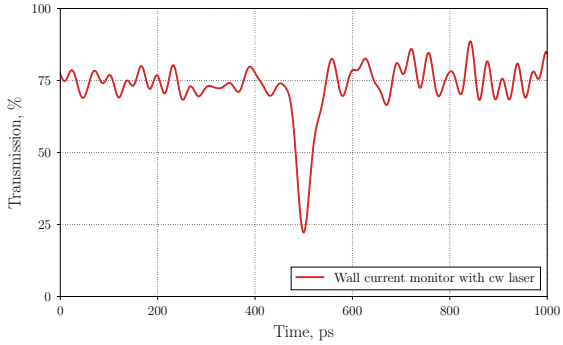

Figure 3: Single-shot measurement using a continuous wave laser (25 mW, 780 nm) as the optical carrier, with a wall current monitor serving as the electrical input. The measurement was conducted at CLEAR with a 200 MeV, 5 ps (1σ), 100 pC electron bunch.

to this bias point. The quadrature point is chosen for its largest sensitivity and highest modulation linearity. When operating the modulator under these conditions, input signals with amplitudes around $V_{\pi/2}$ are saturating the transmitted laser intensity. For input signals with amplitudes exceeding $V_{\pi/2}$, the derivative of the transfer function changes sign, resulting in significant distortions of the output signal. These distortions are known as over-rotation of the output signal.

Continuous Wave Laser

As an intensity modulator is an interferometric device, it is typically used with monochromatic light. In Fig. 3 we present a measurement of a wideband wall current monitor signal [3] obtained using a continuous wave (CW) laser (25 mW, 780 nm), a fast photodetector, and an oscilloscope (Keysight N7004A 33 GHz coupled with a Keysight Infiniium UXR0334A). The measurement was conducted at the CERN Linear Electron Accelerator for Research (CLEAR) [4, 5], using a 200 MeV, 5 ps (1σ), 100 pC electron bunch. The modulator was set to a bias point of 75% and the input signal was attenuated by 33 dB. The single-shot measurement yielded a full width at half maximum (FWHM) of $\tau \approx 37$ ps, corresponding to a bandwidth BW $\approx (2\tau)^{-1} \approx 13.5$ GHz. This bandwidth exceeds the design value of 10 GHz, which has not been achieved previously due to long transmission lines.

Although a system using a CW laser is relatively easy to set up, it has several disadvantages. Firstly, the laser power is distributed continuously over time, while the measured signal occurs only during a brief interval. This leads to the requirement of rather high laser powers to achieve sufficient power densities. Secondly, the optical signal must be read out in real-time using fast electronics, which is often not the most cost-effective solution. Therefore, this work focuses on using pulsed lasers instead.

PULSED LASER SETUP

Switching from a CW laser to a pulsed laser system addresses the two main disadvantages of the CW laser: low power density and the need for fast readout electronics. A schematic of the setup based on laser pulses is shown in Fig. 4. The system uses short laser pulses ($\tau_0 < 130$ fs, center wavelength 780 nm) that pass through a delay stage, a grating stretcher and a pulse picker before being launched into a polarisation-maintaining fibre. The grating stretcher is designed to give anomalous dispersion that partially compensates for the normal dispersion in the approximately 90-meter-long fibre, while the pulse picker reduces the repetition rate from 75 MHz to 10 Hz. The normal dispersion in the fibre alters the chirp direction within the laser pulse, resulting in longer wavelengths arriving earlier in time. The laser pulse is then modulated with a beam-induced electrical signal, which is encoded as an intensity variation on the laser pulse. The laser pulse energy was around 24 pJ at the beginning and around 0.3 pJ at the end of the photonic time stretch setup. Higher pulse energies would improve signal-to-noise ratio. Typically, femtosecond lasers provide pulse energies on the order of nanojoules (nJ) rather than picojoules (pJ), indicating a significant potential for system improvement [6].

Laser Pulse Stretching

The laser pulses must be stretched to a temporal duration longer than the RF signal to be acquired. However, there is a trade-off between stretching and resolution. For a diffraction-limited laser pulse with a Gaussian profile, when stretched from an initial duration τ_0 to a chirped length τ_c, the temporal resolution τ_r is limited by [7]:

$$\tau_r = \sqrt{\tau_0 \tau_c} \tag{3}$$

For an initial pulse duration of $\tau_0 \approx 130$ fs and a chirped pulse duration of $\tau_c \approx 72$ ps at the modulator's location, the shortest pulse duration than can be measured without any distortion is $\tau_r \approx 3.1$ ps. This corresponds to a bandwidth of over 160 GHz. This is much higher than the bandwidth of the modulator to be tested, which typically has a bandwidth of a few tens of GHz.

ISBN: 978-3-95450-249-3 ISSN: 2673-5350 doi: 10.18429/JACoW-IBIC2024-WEAI2

After being encoded onto the laser pulse, the chirp within the pulse enables various decoding techniques. In this work, decoding is performed using either spectral decoding or photonic time stretch.

Spectral Decoding

The spectral decoding technique relies on analysing the spectral content of the chirped laser pulse [8]. The encoded laser pulse is launched into free space using a collimator and then passes a beam expander, which also provides spatial filtering. After being diffracted by a grating, the spectrum is captured with a gated intensified camera. The conversion from pixel position to time is achieved using the delay stage shown in Fig. 4, which delays the laser pulse relative to the beam-induced signal. The conversion factor obtained was 400 ± 3 fs/position, corresponding to a sampling rate of approximately 2500 GS/s. Further details about the spectrometer setup are provided in [9].

Photonic Time Stretch

The photonic time stretch technique involves further stretching the chirped laser pulse in a 600-meter-long fibre. The stretched pulse is then captured by a photodetector and an oscilloscope (Keysight N7004A 33 GHz, coupled with a Keysight Infiniium UXR0404A). The conversion factor, determined using the delay stage, was 432 ± 2 fs/position, corresponding to a sampling rate of approximately 2315 GS/s. Given the oscilloscope's sampling rate of 256 GS/s this results in a stretching factor of approximately 9.

Bias Point Stability

Since the bias point critically influences the modulated signals, it is essential to carefully monitor its stability. Figure 6 illustrates the deviation from the average laser power before and after the modulator. The black curve represents the deviation from the average laser power before the modulator, which was around ±0.5 %. The red curve was obtained after the laser light passed through the modulator at its most sensitive point, corresponding to 50 % transmission. The average power after the modulator fluctuated by a maximum of about ±1.0 % over several hours. It is important to note that this measurement was conducted without any active feedback. Instead, the modulator was allowed to acclimate to its environment for several hours before the measurements were taken.

MEASUREMENTS

First, the signal amplitude must be adjusted to match the dynamic range of the modulator. This was achieved by gradually increasing the charge of the bunches (170 MeV, < 1 ps (1 σ), which in return linearly increases the coherent transition radiation signal. The horn antenna was positioned to produce a bipolar pulse in the modulator, rather than a unipolar one (as compared to the unipolar pulse response in [9]), allowing simultaneous monitoring of the positive and negative signal amplitudes. Figure 7 shows the bipolar pulse

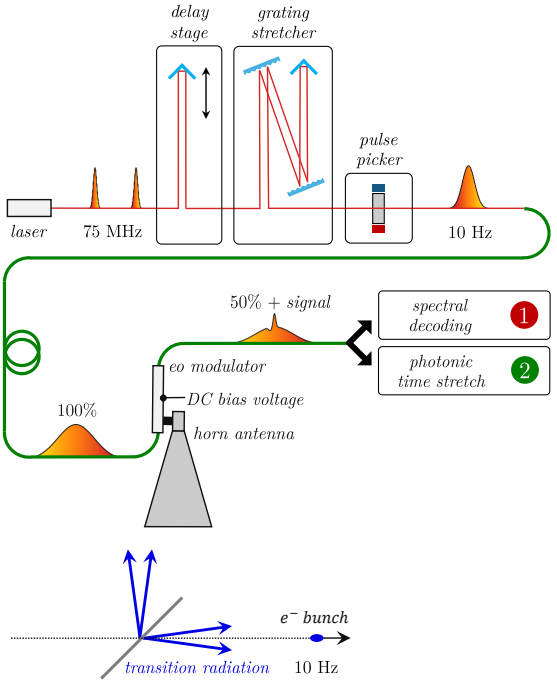

Figure 4: Schematic of the pulsed laser setup. The electrical signal is encoded as an intensity variation on a chirped laser pulse. Decoding is performed either through spectral decoding or photonic time stretch (see Fig. 5 below)

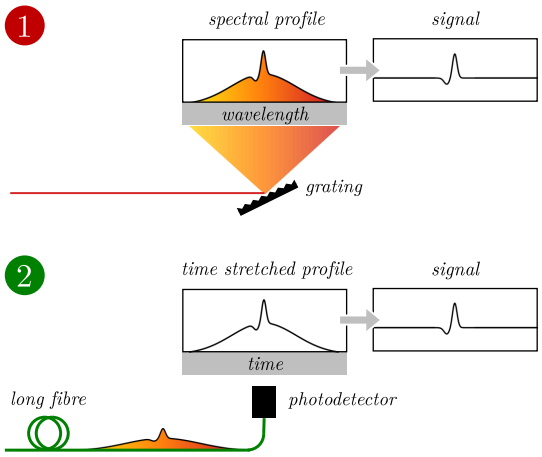

Figure 5: Schematic of the decoding process using the spectral decoding (1) or photonic time stretch (2) technique.

for different bunch charges, with darker colours indicating higher bunch charges.

By analysing the signal amplitude at the positive peak (around 500 ps) and the negative peak (around 525 ps), the transfer function of the modulator can be reconstructed, as shown in Fig. 8. The slight offset of 2.2 ± 0.5 pC can be attributed to the noise floor of the beam current monitor, which was measured at 2.1 ± 1.5 pC. For bunch charges below 9 pC, the underestimation of the signal amplitude is less than 3% relative to the full modulation range.

In Fig. 9 the comparison between the spectral decoding measurement (red curve) and the photonic time stretch mea-

ISBN: 978-3-95450-249-3 ISSN: 2673-5350 doi: 10.18429/JACoW-IBIC2024-WEAI2

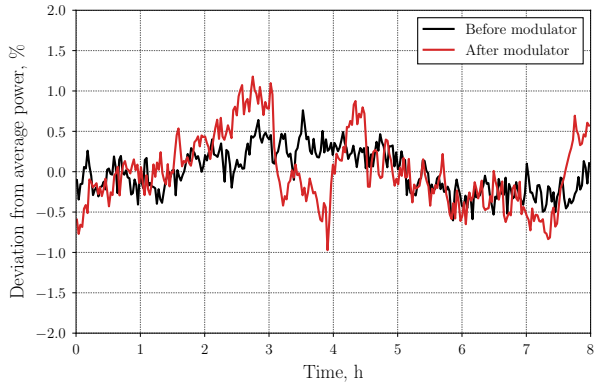

Figure 6: The deviation from the average power is plotted before (black curve) and after (red curve) passing through the modulator at its most sensitive bias point. The measurements were acquired consecutively, so there is no direct correlation between the two curves.

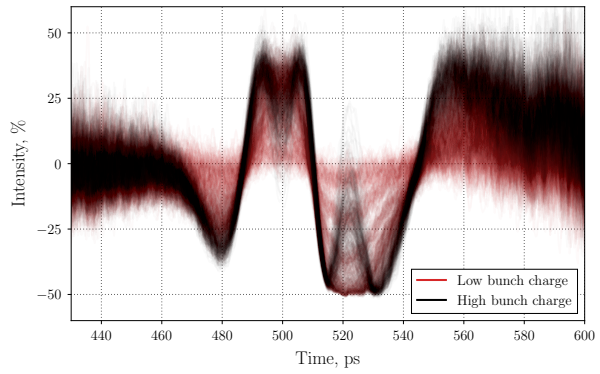

Figure 7: Spectral decoding measurement of coherent transition radiation at different bunch charges. At higher bunch charges (black traces), the transfer function of the modulator saturates, leading to over-rotation of the output signals at the maximum (around 500 ps) and minimum (around 525 ps).

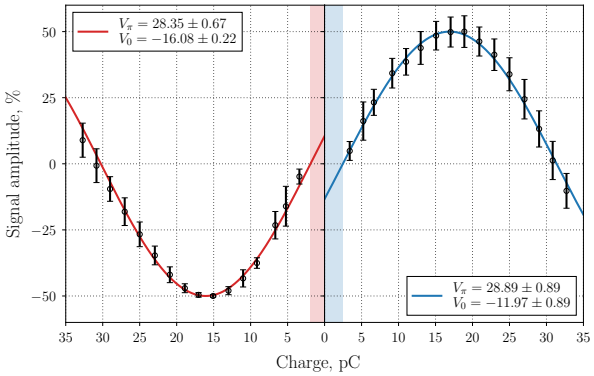

Figure 8: Signal amplitude as a function of bunch charge. The data were extracted from Fig. 7. The blue curve represents the amplitude at maximum signal levels (around 500 ps), while the red curve shows the amplitude at minimum signal levels (cf. 525 ps).

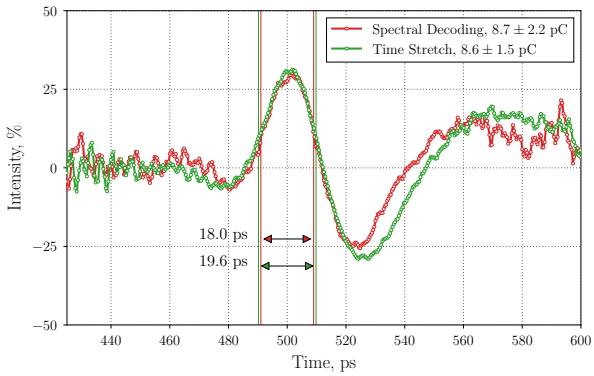

Figure 9: Comparison between spectral decoding (red) and photonic time stretch read-out (green) for an average of 50 acquisitions. Signal amplitudes are scaled based on their averaged bunch charge, following the transfer function measured in Fig. 8.

surement (green curve) is presented, with each curve representing the average of 50 acquisitions. The FWHM of the positive peak is below 20 ps for both measurements, indicating a bandwidth of at least 25 GHz. It should be noted that neither measurement is corrected for timing jitter between the probe pulse and electron bunches. This jitter, estimated using the spectral decoding setup (which is independent of any acquisition jitter caused by external triggering), was found to be $\sigma_t < 2.8$ ps.

To better estimate the modulator bandwidth, single-shot measurements were acquired using both acquisition systems. A bipolar pulse was used, and the signal amplitude was increased to saturate the modulator's transfer function, thereby triggering the steepest fall time the modulator can achieve (see Fig. 10). The 90% to 10% fall time was measured as $t_f < 7.0$ ps for both acquisition methods, corresponding to a bandwidth of approximately BW $\approx 0.35/t_f > 50$ GHz. Additionally, using the slew rate SR of the same signals $SR \geq 2\pi\, V(q) f_{max}$, where $V(q)$ is derived from the input voltage amplitude estimated from the bunch charge, we calculate a maximum frequency $f_{max} \geq 45$ GHz for both acquisition systems.

In the spectral decoding technique dark counts are negligible compared to the photons forming the signal. However, the photodetector in the time stretch setup exhibits a significant noise floor. Figure 11 presents a single-shot measurement of a coherent Cherenkov diffraction radiation signal [10] in two scenarios. The grey line represents the background-removed signal, scaled for the laser envelope amplitude, which reflects the final measurement. The green line shows the background-removed signal without any amplitude correction applied. During this measurement, the modulator was operated at a 20 % bias point, and the background-removed data had a signal-to-noise ratio $S/N > 10$ for a single-shot acquisition. The noise level in the grey curve is elevated due to the fading power of the carrier laser pulse with $\tau_c \approx 72$ ps.

ISBN: 978-3-95450-249-3 ISSN: 2673-5350 doi: 10.18429/JACoW-IBIC2024-WEAI2

DISCUSSION AND CONCLUSION

Electro-optical modulators have proven to be a versatile tool for acquiring fast signals generated in particle accelerators. Various radio-over-fibre techniques were explored, ranging from straightforward systems using CW lasers with fast read-out electronics, to more advanced pulsed laser systems that enable the application of various time stretch techniques. The typically low V_π voltage makes the modulator highly sensitive, necessitating careful adjustment of the input signal amplitude. Both decoding techniques yielded comparable results. Spectral decoding benefits from the absence of acquisition jitter, while photonic time stretch is generally better suited for high repetition rates. The modulator's bandwidth was shown to exceed 45 GHz, surpassing the datasheet value of 25 GHz.

Radio-over-fibre techniques provide the significant advantage of transmitting high-bandwidth signals over long distances. In the context of pulsed signals used in particle accelerators, a pulsed laser setup with electro-optical modulators could effectively address the challenges of transmitting signals in the tens of GHz range. The radiation hardness of current single-mode fibres provides a positive outlook for future radiation-hard polarisation-maintaining fibres, as needed in intensity modulators. Additionally, in large-scale facilities, space for signal transmission is often limited, making optical fibres a more compact alternative to traditional cables. However, for permanent installations, it is essential to thoroughly investigate and test the radiation hardness of the modulators themselves to ensure reliable performance.

ACKNOWLEDGEMENTS

The authors would like to thank the CLEAR operation team for providing the various electron beams used in the presented measurements. We also would like to thank P. Karataev for sharing his expertise and equipment.

This work was supported by the European Union's Horizon 2020 Research and Innovation Programme under grant no. 951754 (FCCIS).

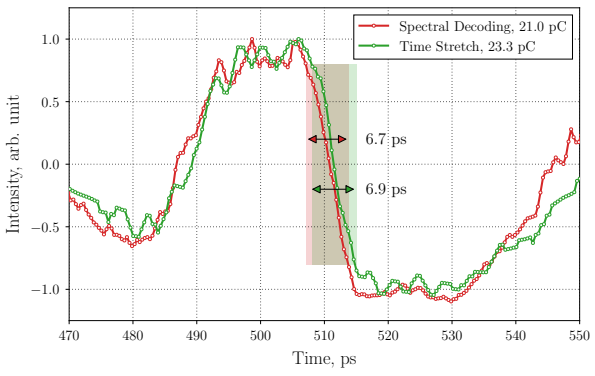

Figure 10: Single-shot measurement of a saturated signal used to estimate the modulator's bandwidth. The bandwidth is determined by the fall time (see graph) or the slew rate of the acquired signals.

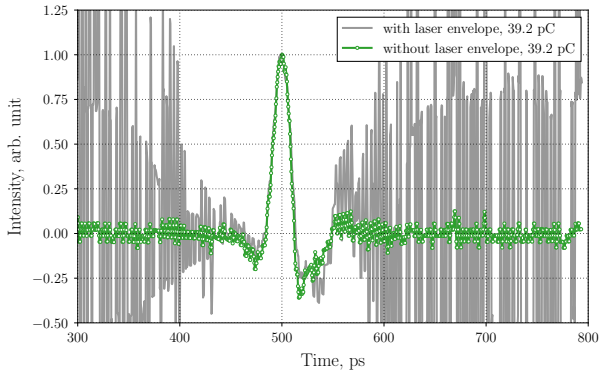

Figure 11: Single-shot measurement using the time stretch method with a coherent Cherenkov diffraction radiation signal and the modulator at a 20% bias point. The averaged background laser pulse signal was subtracted for both measurements. The grey curve shows the amplitude scaled by the laser envelope, while the green curve presents the same data without scaling.

REFERENCES

[1] E.H. Turner, "High-frequency electro-optic coefficients of lithium niobate", *Appl. Phys. Lett.*, vol. 8, no. 11, pp. 303-304, 1966. doi:10.1063/1.1754449

[2] *RF Photonic Technology in Optical Fiber Links*, W.S.C. Chang, Ed. Cambridge University Press, 2002. doi:10.1017/CBO9780511755729

[3] P. Odier, "A new wide band wall current monitor", in *Proc. DIPAC'03*, Mainz, Germany, May 2003, paper PT20, pp. 216–218.

[4] D. Gamba *et al.*, "The CLEAR user facility at CERN", *Nucl. Instrum. Methods in Phys. Res., Sect. A*, vol. 909, pp. 480–483, 2018. doi:10.1016/j.nima.2017.11.080

[5] R. Corsini *et al.*, "First Experiments at the CLEAR User Facility", in *Proc. IPAC'18*, Vancouver, BC, Canada, Apr.–May 2018, pp. 4066–4069. doi:10.18429/JACoW-IPAC2018-THPMF014

[6] C. Szwaj *et al.*, "High sensitivity photonic time-stretch electro-optic sampling of terahertz pulses", *Rev. Sci. Instrum.*, vol. 87, p. 103111, 2016. doi:10.1063/1.4964702

[7] F.G. Sun, Z. Jiang, and X.-C. Zhang, "Analysis of terahertz pulse measurement with a chirped probe beam", *Appl. Phys. Lett.*, vol. 73, pp. 2233–2235, 1998. doi:10.1063/1.121685

[8] I. Wilke *et al.*, "Single-Shot Electron-Beam Bunch Length Measurements", *Phys. Rev. Lett.*, vol. 88, p. 124801, 2002. doi:10.1103/PhysRevLett.88.124801

[9] A. Schlögelhofer, "Non-invasive Beam Diagnostic Development for FCC using Cherenkov Diffraction Radiation in Dielectric Materials", Ph.D. thesis, Phys. Dept., TU Wien, Vienna, Austria, 2024. http://cds.cern.ch/record/2897701

[10] A. Schlögelhofer *et al.*, "Characterisation of Cherenkov Diffraction Radiation Using Electro-Optical Methods", in *Proc. IBIC'23*, Saskatoon, Canada, Sep. 2023, pp. 226–229. doi:10.18429/JACoW-IBIC2023-TUP022